Behavior of a hemp-based concrete wall under dynamic thermal and hygric solicitations

Billy Seng, Camille Magniont, Sandra Gallego, Sylvie Lorente

▶ **To cite this version:**

Billy Seng, Camille Magniont, Sandra Gallego, Sylvie Lorente. Behavior of a hemp-based concrete wall under dynamic thermal and hygric solicitations. Energy and Buildings, 2021, 232, pp.110669. ⟨10.1016/j.enbuild.2020.110669⟩. ⟨hal-03154608⟩

HAL Id: hal-03154608

https://insa-toulouse.hal.science/hal-03154608v1

Submitted on 2 Jan 2023

HAL is a multi-disciplinary open access archive for the deposit and dissemination of scientific research documents, whether they are published or not. The documents may come from teaching and research institutions in France or abroad, or from public or private research centers.

L'archive ouverte pluridisciplinaire **HAL**, est destinée au dépôt et à la diffusion de documents scientifiques de niveau recherche, publiés ou non, émanant des établissements d'enseignement et de recherche français ou étrangers, des laboratoires publics ou privés.

Distributed under a Creative Commons CC BY-NC 4.0 - Attribution - Non-commercial use - International License

Version of Record: https://www.sciencedirect.com/science/article/pii/S0378778820334551
Manuscript_39fecf947bb7e9c771bbb82c338a114e

Behavior of a hemp-based concrete wall under dynamic thermal and hygric solicitations

Billy Seng[1], Camille Magniont[1], Sandra Gallego[1], Sylvie Lorente[1,2,]

[1] LMDC, INSA/UPS Génie Civil, 135 Avenue de Rangueil, 31077 Toulouse, France.

[2] Mechanical Engineering Department, Villanova University, Villanova, PA, USA.

* Corresponding author: sylvie.lorente@villanova.edu

Abstract

Here we document the behavior at wall scale of a hemp-based hygroscopic material under various temperature and moisture dynamic conditions. The wall was made of precast hemp concrete (HC) blocks with air cavities. It was tested within a bi-climatic chamber and monitored thanks to hygrothermal sensors in the wall and in the chambers. The results from an in-house heat and moisture transfer model were compared to the experimental data, using the actual thermal and hygric characteristics of the hemp-based material determined in a previous study. The experiments allowed to demonstrate how the heat and moisture transport phenomena within the wall are coupled, particularly how a temperature difference can be a sufficient driving force for the release of moisture. The work points out the impact of moisture adsorption on heat release and on the temperature changes within the wall. Finally the numerical model served also to the modelling of an equivalent wall made of concrete to help highlighting the moisture dumping capability of the bio-based material, together with its thermal insulation capacity.

Keywords: heat and moisture transfer, bi-climatic chamber, wall scale, Hemp Concrete, bio-based materials.

© 2020 published by Elsevier. This manuscript is made available under the CC BY NC user license
https://creativecommons.org/licenses/by-nc/4.0/

Nomenclature

Latin symbols

A	Aspect ratio	(-)
A_w	Soprtion coefficient	($kg.m^{-2}.s^{-1/2}$)
c_p	specific heat capacity	($J.kg^{-1}.K^{-1}$)
d	air layer thickness	(m)
g	gravitational force	($m.s^{-2}$)
g_m	mass flux	($kg.m^{-2}.s^{-1}$)
h_c	surface heat transfer	($W.m^{-2}.K^{-1}$)
h_m	surface mass transfer	($kg.m^{-2}.s^{-1}.Pa^{-1}$)
H	height	(m)
k	thermal conductivity	($W.m^{-1}.K^{-1}$)
L	length	(m)
L_v	latent heat	($J.kg^{-1}$)
Nu	Nusselt number	
p_c	capillary pressure	(Pa)
p_v	vapor pressure	(Pa)
$p_{v,sat}$	saturated vapor pressure	(Pa)
q_c	heat flux	($W.m^{-2}$)
Ra	Rayleigh number	
RH	relative humidity	(-)
S_l	moisture source term	($kg.m^{-3}.s^{-1}$)

T	temperature	(°C or K)
t	time	(s)
$\boldsymbol{V}$	velocity	(m.s^{-1})
w	total mass water content	(kg.m^{-3})
W	width	(m)

Greek symbols

α	thermal diffusivity	(m^2.s^{-1})
β	thermal expansion coefficient	(K^{-1})
δ	permeability	(kg.m^{-1}.s^{-1}.Pa^{-1} or s)
ν	kinematic viscosity	(m^2.s^{-1})
ρ	density	(kg.m^{-3})

Subscripts

$_f$	free saturation
$_{HC}$	Hemp Concrete
$_i$	liquid or vapor
$_l$	liquid
$_s$	solid
$_{\mathrm{surf}}$	surface
$_v$	vapor

1 Introduction

Hemp Concrete (HC) belongs to the class of bio-based construction materials. It is made of the combination of hemp shiv particles with a binder, generally based on lime in order to maintain the hygroscopic properties of the resulting material. Hemp shiv is the woody core of the hemp stalk obtained through defibration by a mechanical breaking process. The terminology HC is typically used as an analogy to the usual concrete blocks used in construction. Nevertheless, one has to keep in mind that the basic component of concrete, cement, is not present within the HC composition.

Thanks to photosynthesis, bio-based materials can be called CO_2 storage materials. This characteristics, together with the hemp hygrothermal properties developed thanks to the hemp pore structure, make the HC an excellent candidate for meeting sustainable construction objectives. Such materials are perceived as potential solution for energy efficient buildings with a reduced carbon footprint. Controlling heat and moisture transfer through the buildings envelope by using hygroscopic materials may bring a contribution not only on an energy point of view (Osanyintola and Simonson, 2006, Woloszyn et al., 2009) but also on a health standpoint. The increase in moisture content comes indeed with a rise in microorganism concentration (Baughman and Arens, 1996), and the control of mold is directly related to the humidity level in the buildings envelope.

The research field on bio-based construction materials is very active, both on the experimental side and on the modelling one. As far as the latter is concerned, heat and moisture numerical models rely on different driving potentials to describe the moisture exchanges: it can be either the moisture content or the capillary pressure or the vapor pressure. Therefore the final set of

88 equations varies from one author to another one. Examples of models can be found in the works
89 Hagentoft et al. (2004), Li et al. (2009), Tariku et al. (2010), Steeman et al. (2010), Delgado et al.
90 (2013), or Van Belleghem et al. (2014). The main modelling challenge lies in the fluid flow
91 through the porous structure combined to phase change, making the set of equations to solve
92 highly non-linear. The issue is highlighted in Souza et al. (2008), Mahabaleshwar et al. (2017),
93 Salimpour et al. (2017), Husman et al. (2016), Pepe et al. (2017).

94 The experimental investigations rang from the sample scale to the building scale in real climatic
95 conditions. For example, detailed measurements were presented in Lelievre et al. (2014) on a
96 hemp-based element showing the thermo-hygric response to a change of relative humidity of the
97 environment. Wall scale laboratory experiments were performed by Aït Oumeziane et al. (2016)
98 in almost isothermal conditions. In 2018, Moujalled et al. published the results of an
99 experimental campaign of 4 years on a house which envelope was partially made of a sprayed
100 hemp and lime concrete, demonstrating the moisture buffering capacity of such material in real
101 life climatic conditions. This work came after the pioneering works of Shea et al. (2012)
102 performed on a rather smaller building based on different construction techniques.

103

104 The work presented in this paper is aimed at investigating the response of a wall made of a hemp-
105 based material to controlled dynamic solicitations in both temperature and humidity within a bi-
106 climatic chamber. The temperature and water vapor profiles obtained during the experimental
107 campaign serve a three-fold purpose: one is to assess the moisture buffering capacity of such
108 material, the other is to provide a set of HAM (Heat and Moisture) data necessary to the wall-
109 scale validation of a numerical model based on the finite elements method; the final one is to

examine how the hemp-based wall behavior differentiates from a classical concrete wall in terms of thermo-hygric response.

2 Experiments

2.1 Hemp Concrete wall in the test chamber and metrology

Blocks of HC were assembled in order to constitute a wall of 2.3 m in height, 1.6 m in width and 20 cm in thickness. Each HC block had the following dimensions: length = 50.8 ± 1.04 cm, thickness = 19.9 ± 0.09 cm, height = 20.3 ± 0.24 cm. The assembly was made thanks to thin horizontal mortar layers (70% metakaolin and 30% hydrated lime, sand/binder = 5 and water/binder = 0.6), while the vertical sides of the blocks were interlocked to each other (see Fig. 1 for the geometric features). The HC blocks contain air cavities (Fig. 1a). Due to the vibro-compaction fabrication process, the HC layers were slightly thicker at the bottom of the brick (HC thickness = 2.55 ± 0.07 cm at the top of the brick against 2.72 ± 0.09 cm at the bottom) while it was the opposite for the air layer (air thickness = 0.94 ± 0.07 cm at the top against 0.71 ± 0.06 cm at the bottom). Mean values of HC layer thickness (2.63 ± 0.08 cm) and air layer thickness (0.82 ± 0.07 cm) were considered in the numerical study.

The HC was initially characterized by measuring its physical, thermal and hygric properties: density, porosity, thermal conductivity, specific heat capacity, air and vapor permeability, sorption and desorption isotherms, capillary adsorption coefficient. The details of this work can be found in Seng et al. (2019a, 2019b) and were used here as input data in the numerical model. The relationship between the relative humidity and the moisture content is an important topic as in most cases hemp-based materials exhibit a strong hysteretic behavior between adsorption and desorption, while the temperature at which the sorption-desorption isotherm experiments are

conducted may also have impact (Aït Oumeziane et al., 2016). The results corresponding to the HC tested in this study are provided in Fig. 2, showing that the sorption and desorption measurements at 23°C and 45°C gather along one single curve, justifying the use of a unique isotherm in the study.

Insert Figure 1

Insert Figure 2

The test environment was made of two climatic rooms; both were controlled in temperature and relative humidity. Each room has a horizontal surface of L x W = 3.30 m x 1.60 m and a height of H = 2.30 m. The HC wall was placed into a wooden frame in order to separate the two chambers. Special attention was dedicated to avoid any humid air leakage through the frame or the wall-frame interface. Note that deflectors were installed so that the air blown into the chambers to maintain the chosen boundary conditions was not directly oriented toward the wall.

The hygrothermal behavior of the HC wall was monitored with 10 hygrothermal sensors (Honeywell HIH-4602-C). Each hygrothermal sensor was equipped with a 2 wires integral precision RTD sensor for the temperature (precision: Class B, ±0.3 +0.005T °C), and a planar capacitor for the RH (± 3.5% RH).

The hygrothermal sensors were distributed along the thickness of the wall, at the wall mid-height, in the air cavities inside the wall and against the wall (Fig. 3). One sensor was deported horizontally (sensor 7) so that the one-dimensional aspect of the transfer could be checked. All the sensors were connected to a data acquisition processor which returned the measurements to a computer outside the bi-climatic chamber.

Insert Figure 3

2.2 Tests summary

A first series of test consisted in measuring the hygrothermal response of the wall to a temperature step solicitation without any moisture exchange between the wall and its surrounding environment. To this sake, the 2 faces of the wall were coated with a vapor barrier. After an initial stabilization phase at 25°C in the 2 rooms, the temperature was steeply increased to 45°C on one side, and maintained to this value for about 4 days.

In a next series, one chamber represented outdoor conditions, while the opposite one (hot side) was meant to reproduce indoor conditions. The hot side was always maintained at a constant temperature. In one case, vapor was produced for 1 hour in order to model room occupancy; the cold side was kept at 6°C and RH = 80%. The test lasted about 4 days. In the other case, the cold chamber was submitted to a sinusoidal temperature signal with an average temperature of 14°C, a total temperature amplitude of 16°C and a period of 24 hours. The RH slightly fluctuated around

172 80%. The hot chamber RH was not controlled. The test lasted 6 days. Figure 4 summarizes the 3
173 configurations.

174 Insert Figure 4

175 3 Numerical study

176 3.1 Heat and moisture transfer through the HC

177 The problem is described by the conservation laws written for the HC layers and for the air
178 layers. Equations (1) to (3) present the moisture transfer, the energy transfer and the moisture
179 phase change rate in time. A first version of the model considering only HC was published in
180 Seng et al. (2017). In this paper the work was compared to experimental data obtained on a small
181 sample of HC from Lelievre et al. (2014). Working with realistic boundary conditions at a much
182 bigger scale with actual wall elements is the aim of the present study.

183 The set of equations was solved for three variables: the capillary pressure p_c, the temperature T
184 and the moisture source term S_l which corresponds to the amount of moisture stored or released
185 in time by the solid phase.

$$\frac{\partial w}{\partial p_c}\frac{\partial p_c}{\partial t} = -\boldsymbol{\nabla}\left[\left(\delta_l + \delta_v \frac{\rho_v}{\rho_l}\right)\boldsymbol{\nabla} p_c - \delta_v \left(\mathrm{RH}\frac{\partial p_{v,sat}}{\partial T} - p_v \frac{\ln \mathrm{RH}}{T}\right)\boldsymbol{\nabla} T\right] \quad (1)$$

$$\left(\rho_s c_{p,s} + \sum_i w_i c_{p,i}\right)\frac{\partial T}{\partial t} = k_{HC}\boldsymbol{\nabla^2} T - \left[\left(c_{p,l} - c_{p,v}\right)T - L_v\right]S_l - \sum_i w_i \boldsymbol{V}_i c_{p,i}\boldsymbol{\nabla} T \quad (2)$$

$$\left(\frac{1}{1 - {\rho_v}/{\rho_l}}\right)\frac{\partial w}{\partial t} = -\boldsymbol{\nabla}(\delta_l \boldsymbol{\nabla} p_c) + S_l \quad (3)$$

where w is the total moisture content, δ_l is the liquid permeability, δ_v is the vapor permeability, ρ_v is the water vapor density, ρ_l is the liquid water density, p_v is the vapor pressure, p_{vsat} is the saturated vapor pressure, ρ_s is the material apparent density, w_i ($i = v$ for water vapor or $i = l$ for liquid water) is the moisture content, $c_{p,i}$ is the specific heat capacity of water vapor or liquid water , k_{mat} is the material thermal conductivity, $\boldsymbol{V}_i$ is the velocity of water vapor or liquid water and L_v is the latent heat of vaporisation.

The HC thermal and hygric properties were measured in Seng et al. (2019a) and Seng et al. (2019b). The curved fitting parameters obtained by means of the GAB model (Anderson, 1946) are provided in Table 1 together with a summary of the other material properties. Note that the amount of transported water vapor or liquid water $w_i\boldsymbol{V}_i$ can be defined by $w_v\boldsymbol{V}_v = -\delta_v\boldsymbol{\nabla}p_v$ and $w_l\boldsymbol{V}_l = \delta_l\boldsymbol{\nabla}p_c$, and that the $\sum_i w_i c_{p,i} \approx w c_{p,l}$ due to the small value of w_v compared to w_l.

3.2 Heat and moisture transfer through the air layers

The Rayleigh number of an air cavity is given by

$$Ra_d = \frac{g\beta\Delta T d^3}{\alpha\nu} \tag{4}$$

where g is the gravitational force, β is the thermal expansion coefficient written $\beta = 1/T$ as air was considered as an ideal gas, ΔT is the temperature difference between the two faces of the cavity, d is the air layer thickness, α is the air thermal diffusivity and ν is the air kinematic viscosity.

It was assumed that the temperature difference ΔT within an air layer varies from 1°C to 5°C. The Rayleigh number based on d, Ra_d estimated with Eq. (4) was therefore lower than 300. With an air layer thickness d = 0.82 cm, the air cavity aspect ratio is $A = H/d = 24.8$, with H = 20.3 cm. As $Ra_d < 10^4$ and $5 \leq A \leq 80$, the Nusselt was evaluated with the expression provided by Zhao et al. (1997):

$$Nu = \left(1 - 0.00813277\left(\frac{Ra_d}{\mathrm{A}}\right) + 0.00723291\left(\frac{Ra_d}{\mathrm{A}}\right)^{1.08597}\right)^{0.279072} \quad (5)$$

Because $Nu \leq 1$, only conductive transfer was considered through the air cavity. With no convective transfer effect and no liquid phase transfer in the air cavity, the resulting HAM equations are:

$$\frac{\partial w_{air}}{\partial p_c}\frac{\partial p_c}{\partial t} = -\boldsymbol{\nabla}\left[\left(\delta_v \frac{\rho_v}{\rho_l}\right)\boldsymbol{\nabla} p_c - \delta_v\left(\mathrm{RH}\frac{\partial p_{vsat}}{\partial T} - p_v\frac{\ln \mathrm{RH}}{T}\right)\boldsymbol{\nabla} T\right] \quad (6)$$

$$\left(\rho_{air} c_{p,air} + w_v c_{p,v}\right)\frac{\partial T}{\partial t} = k_{air}\boldsymbol{\nabla^2} T \quad (7)$$

$$S_l = 0 \quad (8)$$

where w_{air} is the water vapor content in air defined from the ideal gas law (Table 1).

Table 1 : HC and air properties used in the numerical study

Parameter	Hemp Concrete (from Seng et al., 2019a, Seng et al. 2019b)	Air

Density	ρ_{HC} = 466.2 kg.m^{-3}	ρ_{air} = 1.2 kg.m^{-3}
Thermal conductivity	k_{HC} = 0.112 W.m^{-1}.K^{-1}	k_{air} = 0.026 W.m^{-1}.K^{-1}
Specific heat capacity	$c_{p,HC}$ = 905 J.kg^{-1}.K^{-1}	$c_{p,air}$ = 1004 J.kg^{-1}.K^{-1}
Isotherm	GAB model $w_{HC} = \frac{\rho_{HC} \cdot u_m \cdot C \cdot K \cdot RH}{(1 - K \cdot RH)(1 + K(C-1)\mathrm{RH})}$ u_m 0.0182 C 18.048 K 0.8219 (NB: the curve-fitting parameters correspond to a temperature of 23°C in adsorption)	Water vapor considered as an ideal gas $w_{air} = \frac{RH \cdot p_{v,sat}(T)}{R_v T}$ where R_v is the water vapor specific gas constant ($R_v = R/M_v$) R = 8.314 J.mol^{-1}.K^{-1} M_v = 18 10^{-3} kg.mol^{-1}
Water vapor permeability	$\delta_{v,HC}$ = 9.67 10^{-11} kg.m^{-1}.s^{-1}.Pa^{-1}	$\delta_{v,air}$ = 1.95 10^{-10} kg.m^{-1}.s^{-1}.Pa^{-1}
Liquid permeability	$\delta_{l,HC} = D_w \frac{\partial w}{\partial RH} \frac{RH}{\rho_l R_v T}$ where $D_w = 3.8 \left(\frac{A_w}{w_f}\right)^2 1000^{\frac{w}{w_f}-1}$ A_w = 0.139 kg.m^{-2}.s$^{-1/2}$ w_f = 541 kg.m^{-3}	$\delta_{l,air}$ = 0 kg.m^{-1}.s^{-1}.Pa^{-1}

3.3 Boundary conditions

The thermal boundary conditions between the wall and the air in the climatic chambers were described with a convective heat flux q_c (W.m^{-2}) in which the chamber temperature, T_{air}, may vary in time.

$$q_c = h_c(T_{surf} - T_{air}) \quad (9)$$

where h_c is the convective heat transfer coefficient.

The hygric boundary conditions were given by a convective mass transfer flux g_m, in which h_m is the convective mass transfer coefficient.

$$g_m = h_m(p_{v,surf} - p_{v,air}) \quad (10)$$

The convective heat transfer coefficient was determined based on the air velocity v_{air} (m.s^{-1}) using a correlation of NF EN 15026 (AFNOR, 2008). The convective mass transfer coefficient was established with the heat and mass transfer analogy used by the same reference.

The air velocity was measured in the bi-climatic chamber; the corresponding convective heat and mass transfer coefficients are given in Table 2.

Table 2: Convective heat and mass transfer coefficients

Cold chamber	Hot chamber
v_{air}= 5.3 m.s^{-1} h_c= 23.5 W.m^{-2}.K^{-1} h_m= 1.21 10^{-7} (kg.m^{-2}.s^{-1}.Pa^{-1}).	v_{air}= 5.1 m.s^{-1} h_c= 22.85 W.m^{-2}.K^{-1} h_m= 1.18 10^{-7} (kg.m^{-2}.s^{-1}.Pa^{-1}).

3.4 Numerical procedure

The model based on Eqs. (1)-(3) and Eqs. (6)-(8) was implemented in a FEM software, using the Partial Differential Equations module (COMSOL, 2017). The boundary conditions were set according to Eqs. (9) and (10): the air temperature and vapor pressure came from the measurement in the middle of the chamber (sensor 1 and 10, see Fig.3). A mesh sensitivity was performed this way: the maximum element size was set initially to 4 mm (corresponding to 114

236 elements) and divided by two one run after the other. We observed the temperature and the
237 capillary pressure in the positions corresponding to the sensors shown in Fig.3. The error from
238 one mesh to the other one was lower than 2.5% when the maximum element size was 0.25 mm
239 which corresponded to 808 elements. We selected the case with the next step mesh refinement,
240 i.e. with elements of maximum 0.125 mm leading to a mesh of 1600 elements.

241 At the interface between HC and air cavity, we considered temperature and capillary pressure
242 continuity (Eqs. (11) and (12)).

$$T_{air} = T_{HC} \tag{11}$$

$$p_{c,air} = p_{c,HC} \tag{12}$$

243

244 4 Results and Discussions

245 4.1 Moisture exchange potential

246 The experimental results obtained in the presence of the vapor barriers are presented in Fig. 5
247 together with the simulations results after 1, 12 hours and 90 hours. The temperature and vapor
248 pressure measured at the start of the test were used as initial conditions in the numerical model.
249 One hour after the right-hand side (hot) chamber temperature was increased to 45°C, a
250 temperature profile typical to heat diffusion was measured within the wall. The conductive heat
251 wave propagated towards the opposite side until a linear temperature profile was reached after
252 about 90 hours.

253 The temperature gradient occurring on the right hand side of the wall comes with a vapor
254 pressure gradient of the same sign. Because the two vapor barriers ensure that no moisture uptake
255 happens from the climatic chambers, the vapor pressure increase in the material was due only to a
256 moisture release from the bio-based material. The desorption of water molecules happened from
257 right to left, and stopped after 90 hours as depicted by the horizontal vapor pressure profile.

258 The release of vapor was activated by the temperature gradient. The temperature profile was
259 almost linear after 12 hours, while it took about 90 hours for the moisture to be released and the
260 water vapor pressure profile to become horizontal. Once the temperature change stopped, the
261 moisture gradient was a strong enough driving force to generate an additional release of vapor by
262 the solid phase towards the left-hand side of the wall.

263 The numerical results reproduce the thermo-hygric behavior with a good accuracy. It is worth
264 pointing out that the numerical temperature profile is the result of heat transfer by conduction
265 through the wall combined to the latent heat contribution that accompanies the release of water
266 molecules by the hemp-based matrix (see Eq. (2)). The scale analysis of heat and moisture
267 transfer conducted in Seng et al. (2017) demonstrated that, for the range of temperature and
268 humidity tested here, the third term in the right-hand side of the energy conservation was
269 negligible.

270

271 Insert Figure 5

272

4.2 Occupancy in winter conditions

This situation corresponds to the presence of an occupant within the right-hand side (hot) chamber for 1 hour leading to a peak in RH while the ambient temperature remained constant. The cold chamber was maintained at 6 °C. Figure 6 shows the temperature and moisture measurements in time on the wall surface (hot chamber side) and within the wall. The ambient conditions (hot chamber) are shown in Fig. 6a, while Fig. 6b and c show the response at respectively about 3 cm (sensor 8) and about 6.5 cm (sensor 6) from the hot surface.

The vapor production happened a little bit before the start of the 3rd day of test. Because the ambient temperatures had been maintained constant on both sides of the wall, the latter was in thermal equilibrium when vapor started to be produced. Yet, Fig. 6b exhibits a temperature bump of about 1°C at 3 cm from the hot surface which cannot be attributed to the thermal conditions. Indeed, the adsorption of molecules of water vapor onto a hydrophilic surface comes with a heat released. The enthalpy of adsorption, which depends on the type of solid surface, generates a temperature increase detected by the sensors. Figure 6 indicates that this exothermic property of water molecules adsorption was well predicted by the numerical model. Moving deeper into the wall, the vapor pressure peak continued to appear but with a time lag: the increase in vapor pressure and temperature was detected by the sensor at 3cm in the wall as soon as vapor was produced in the hot chamber. A few centimeters deeper into the wall (sensor 6) a bump in vapor pressure and in temperature remains noticeable but more centered towards Day 3, while its amplitude decreased as the bio-based material kept adsorbing moisture. Consequently, as less vapor was adsorbed onto the surface of the hemp fibers, the resulting peak temperature also decreased. The numerical model describes coherently the thermos-hygric behavior even though the temperature evolution in time are 1 °C below the measured values.

296

297 Insert Figure 6

298

299 **4.3 Sinusoidal solicitations**

300 Sinusoidal temperature and moisture solicitations tests are yet another way to assess the dynamic
301 behavior of the HC. The results presented in this section correspond to a moment when a steady
302 periodic regime is established. As shown in Fig. 4c, the sinusoidal temperature in the left-hand
303 side (cold) chamber had a period of 24 hours. The RH was set to slightly fluctuate around 80%.
304 There was a small overall increase of RH along the 6 days of test, around 1% per cycle. The
305 temperature in the hot chamber was maintained at 24°C, and maintained constant throughout the
306 test which lasted one week. The RH was left free to vary in this chamber.

307 The measurements in the 2 chambers are plotted in Fig. 7 in terms of vapor pressure and
308 temperature. Note that in the cold chamber the temperature peaks correspond as expected to the
309 vapor pressure peaks (Fig. 7a). As shown in Fig. 7b, the vapor pressure change in the hot
310 chamber also followed a sine wave in time, but with a much smaller amplitude than the one of the
311 vapor pressure in the cold chamber. This amplitude remained unchanged over the course of the
312 test, the vapor pressure ranging between 1000 and 1445 Pa. The RH corresponding to that
313 evolution was between 34% and 48%. The period was also 24 hours. Moisture was absorbed by
314 the wall, and its peak was detected in the opposite chamber about 4.3 hours after the moisture
315 peak solicitation.

316 Figure 8 provides the temperature and vapor pressure changes in time at 3 different locations
317 within the wall: in the vicinity of the left-hand side (cold) chamber where the ambient was
318 controlled, at mid-distance within the wall, and in the vicinity of the hot chamber. In this figure,
319 all the plain lines correspond to experimental results, while the dotted lines are for the numerical
320 results.

321 The 3 sensors measured a steady periodic response of the temperature within the wall. The
322 amplitude of the sine wave is higher in the vicinity of the cold side, and almost linear next to the
323 opposite side where the ambient temperature was maintained constant.

324 Figure 8 shows how the sinusoidal variation in vapor pressure is transmitted from the cold side to
325 the warm chamber. The vapor pressure flow goes from the cold side to the hot one, as a sine
326 wave which amplitude decreases while approaching the hot chamber, as indicated by the
327 experimental values. Because only the cold chamber was controlled in relative humidity, a wall
328 made of a material with less hygroscopic properties would let the relative humidity in the hot
329 chamber increase in time. In the case of a wall made of HC, part of the water vapor is trapped
330 within the material and this moisture damping property explains the lower vapor pressure
331 amplitude on the hot side.

332 Plotted in Fig. 8 are also the numerical results obtained for the simulation of the HC wall. Note
333 the good agreement between the numerical results and the experimental ones. This final
334 validation of the model allowed to consider with confidence the case of a classical wall made of a
335 material with non-hygroscopic properties with the purpose of differentiating thermal and hygric
336 behaviors.

337 To this sake, we chose to model a wall made of a classic plain concrete. Concrete has a thermal
338 conductivity more than 10 times higher than the HC one, with a similar specific heat capacity. In
339 addition to being more thermally conductive, a typical concrete is also much less hygroscopic.
340 The concrete properties are provided in the EN 15026 norm (AFNOR, 2008). The initial and
341 boundary conditions were identical to the ones used in the modelling of the experiment. The
342 results corresponding to the simulation of the concrete wall were added to Fig. 8. The vapor
343 pressure wave decreases in amplitude when moving from the cold chamber to the hot one. Yet
344 the amplitude is larger than in the case of HC. The concrete wall clearly does not have the same
345 damping property as the hemp-based wall. Figure 8 also highlights the lower moisture buffering
346 capacity of concrete: its peak of vapor pressure is less delayed that for the HC, meaning that the
347 moisture wave travels faster than for the hemp-based wall. As expected, the same result is
348 obtained for heat transfer. Figure 8c shows that the thermal wave is still present in the case of the
349 plain concrete wall in the vicinity of the hot chamber. These results highlights the potential of
350 HC as a material suitable for thermal comfort: relatively to a classical concrete-based wall, the
351 hemp-based wall is able to dampen moisture changes while demonstrating a good thermal
352 insulation.

353 # 5 Concluding remarks

354 In this paper, the hygrothermal behavior of a wall made of precast HC blocks in a bi-climatic
355 chamber was measured in different boundary conditions corresponding to realistic situations. The
356 experimental data were compared to the numerical results obtained from a model based on FEM.
357 The hygrothermal properties of the HC came from the works of Seng et al. (2019a, 2019b). The
358 numerical model, once validated, was used as a comparison tool with a typical wall made of plain

concrete, in the case of a dynamic solicitation in temperature and vapor pressure on one side of the wall. The study highlighted:

- The potential for the hemp-based wall to release moisture under an applied temperature difference while water exchange with the ambient is prevented.
- The ability to adsorb a sudden peak of humidity from the ambient environment within a few hours,
- The capacity, unlike a concrete-based wall, to dampen a thermal and hygric sinusoidal solicitation, decreasing the moisture wave amplitude from one chamber to the other one, while delaying its travel through the wall.

Acknowledgements:

Billy Seng's PhD thesis was funded by the NeOCampus research project.

Figures caption

Figure 1 (a) HC block, (b) HC wall (built by Vu et al., 2015), and (c) wall instrumented with hygrothermal sensors.

Figure 2 Sorption and desorption isotherm of the HC at 23°C and 45°C, adapted from Seng et al. (2019b).

Figure 3 Hygrothermal sensors in the bi-climatic chamber: (a) side view of the bi-climatic chamber, (b) top view of the sensors installation.

Figure 4 The different experimental configurations: (a) the wall is coated with a vapor barrier on each side and submitted to a temperature difference between the 2 ambiences, (b) 1 hour of vapor production in one chamber simulates the presence of an occupant indoor, the outside is meant to represent winter conditions, and (c) a sinusoidal temperature solicitation with constant RH in the cold chamber while the other chamber is maintained at constant temperature.

Figure 5 Temperature and vapor pressure distribution within the wall when the wall is coated by a vapor barrier on its both sides. (a) initial conditions, after (a) 1 hour, (b) 12h (b) and (c) 90 hours.

Figure 6 Temperature and vapor pressure evolution in time (a) in the hot chamber, (b) at 3 cm and (c) at 6.5 cm from the hot side. The solicitation is meant to resemble the moisture production that an individual would produce during 1 hour of room occupancy. The plain lines are for the experimental results, while the dotted lines correspond to the experimental ones.

Figure 7 Temperature and vapor pressure changes in time in (a) the hot chamber and (b) the cold chamber when the cold side is submitted to sinusoidal temperature with ~ constant RH and the hot side is simply maintained at constant temperature. The plain lines are for the experimental results, while the dotted lines correspond to the experimental ones.

Figure 8 Temperature and vapor pressure changes in time within the material at (a) 3 cm from the cold side, (b) mid wall thickness and (c) 6.5 cm from the hot side, when the boundary conditions are those of Fig. 7. The experimental curves are

completed by the numerical ones in the case of the HC wall and for a similar wall made of concrete. The plain lines are for the experimental results, while the dotted lines correspond to the experimental ones.

REFERENCES

AFNOR. Hygrothermal performance of building components and building elements - Assessment of moisture transfer by numerical simulation, NF EN 15026:2008, 2008, 22p.

Aït Oumeziane, Y., Moissette S., Bart M., Collet F., Pretot S., Lanos C., 2016, Influence of hysteresis on the transient hygrothermal response of a hemp concrete wall, J. Building Performance Simulation, 10 265-271.

Anderson R.B., 1946, Modifications of the Brunauer, Emmett and Teller Equation, J. AM; Chem. Soc., 68 686-691.

Baughman A., Arens E., 1996, Indoor humidity and human health-Part I: Literature review of health effects of humidity-influenced indoor pollutants. ASHRAE Transactions, 102(1) 193–211.

COMSOL, 2017, www.comsol.com

Delgado, J.M.P.Q., Barreira, E., Ramos, N.M.M., de Freitas, V.P., 2013. Hygrothermal Numerical Simulation Tools Applied to Building Physics, SpringerBriefs in Applied Sciences and Technology. Springer Berlin Heidelberg, Berlin, Heidelberg.

Hagentoft, C.-E., Kalagasidis, A.S., Adl-Zarrabi, B., Roels, S., Carmeliet, J., Hens, H., Grunewald, J., Funk, M., Becker, R., Shamir, D., Adan, O., Brocken, H., Kumaran, K., Djebbar, R., 2004. Assessment Method of Numerical Prediction Models for Combined Heat, Air and Moisture Transfer in Building Components: Benchmarks for One-dimensional Cases. Journal of Building Physics 27, 327–352.

Usman, H., Mabood, F., Lorenzini, G., 2016, Heat and Mass Transfer along Vertical Channel in Porous Medium with Radiation Effect and Slip Condition, Int. J. of Heat and Technology, 34, 129–136.

Lelievre, D., Colinart, T., Glouannec, P., 2014. Hygrothermal behavior of bio-based building materials including hysteresis effects: Experimental and numerical analyses. Energy and Buildings 84, 617–627.

Li, Q., Rao, J., Fazio, P., 2009. Development of HAM tool for building envelope analysis. Building and Environment 44, 1065–1073.

Mahabaleshwar, U. S., Basavaraja, D., Wang, S., Lorenzini, G., Lorenzini E., 2017, Convection in a porous medium with variable internal heat source and variable gravity, Int. J. Heat and Mass Transfer, 111, 651–656.

Moujalled B., Aït Oumeziane Y., Moissette S., Bart M., Lanos C., Samri D., 2018, Experimental and numerical evaluation of the hygrothermal performance of a hemp lime concrete building: A long term case study, Building and Environment 136 11-27.

Osanyintola, O.F., Talukdar, P., Simonson, C.J., 2006. Effect of initial conditions, boundary conditions and thickness on the moisture buffering capacity of spruce plywood. Energy and Buildings 38, 1283–1292.

Pepe, V., Rocha, L., Miguel, A., 2017. Optimal Branching Structure of Fluidic Networks with Permeable Walls, BioMed Research International 2017, 5284816.

Salimpour, M.R., Kalbasi, R., Lorenzini, G., 2017. Constructal multi-scale structure of PCM-based heat sinks, Continuum Mechanics and Thermodynamics 29, 477–491.

Seng B., Lorente S., Magniont C., 2017. Scale analysis of heat and moisture transfer through bio-based materials ─ Application to hemp concrete, Energy and Buildings 155 546-558.

Seng B., Magniont C., Lorente S., 2019a. Characterization of a precast hemp concrete. Part I: Physical and thermal properties, *J. Building Engineering*, 24 100540.

Seng B., Magniont C., Lorente S., 2019b. Characterization of a precast hemp concrete. Part II: Hydric properties, *J. Building Engineering*, 24 100579.

Shea, A., Lawrence, M., Walker, P., 2012. Hygrothermal performance of an experimental hemp–lime building. Construction and Building Materials 36, 270–275.

Steeman, M., Janssens, A., Steeman, H.J., Van Belleghem, M., De Paepe, M., 2010. On coupling 1D non-isothermal heat and mass transfer in porous materials with a multizone building energy simulation model. Building and Environment 45, 865–877.

Souza, J, NavaI, M., Rocha, L., Amico, S., 2008, Two-dimensional control volume modeling of the resin infiltration of a porous medium with a heterogeneous permeability tensor, Materials Research 11, 261–268.

Tariku, F., Kumaran, K., Fazio, P., 2010. Transient model for coupled heat, air and moisture transfer through multilayered porous media. International Journal of Heat and Mass Transfer 53, 3035–3044.

Van Belleghem, M., Steeman, M., Janssen, H., Janssens, A., De Paepe, M., 2014. Validation of a coupled heat, vapour and liquid moisture transport model for porous materials implemented in CFD. Building and Environment 81, 340–353.

Vu, T.L., Spagnol, S., Magniont, C., 2015. Experimental study of the hygrothermal behaviour of hemp shives-based precast blocks at material and wall scales. 1st Int. Conf. Bio-based Building Materials (ICBBM), Clermont-Ferrand, France.

Woloszyn, M., Kalamees, T., Olivier Abadie, M., Steeman, M., Sasic Kalagasidis, A., 2009. The effect of combining a relative-humidity-sensitive ventilation system with the moisture-buffering capacity of materials on indoor climate and energy efficiency of buildings. Building and Environment 44, 515–524.

Zhang, H., Yoshino, H., Hasegawa, K., Liu, J., Zhang, W., Xuan, H., 2017. Practical moisture buffering effect of three hygroscopic materials in real-world conditions. Energy and Buildings 139, 214–223.

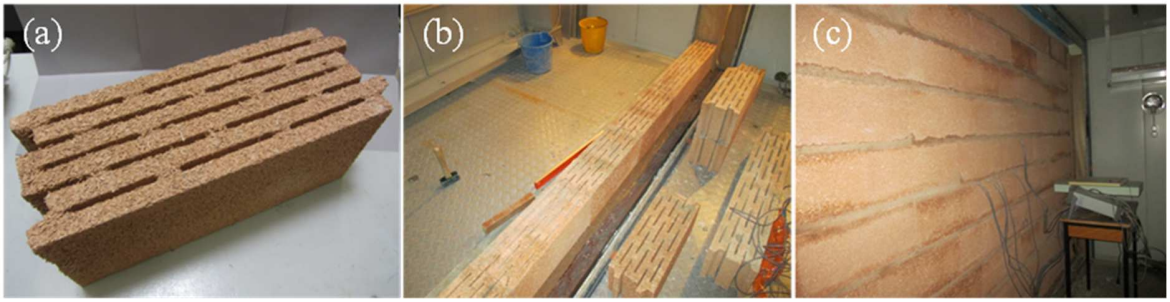

Figure 1

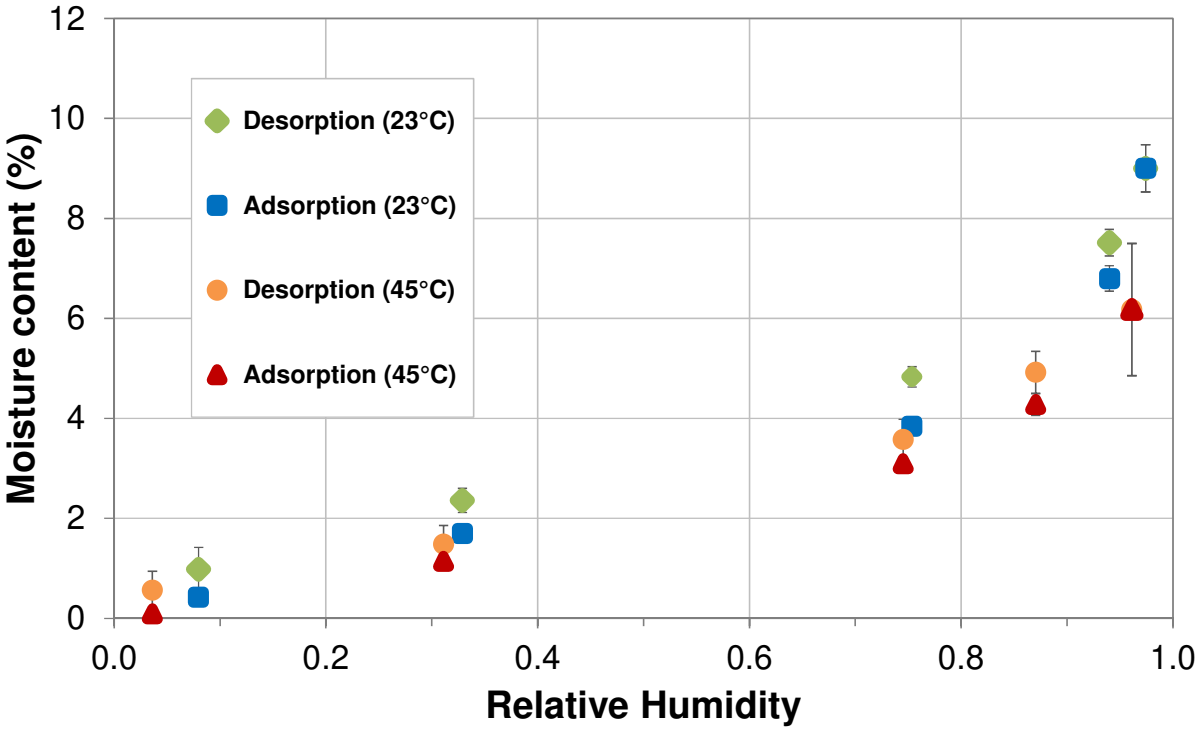
Moisture content (%)
12
10
8
6
4
2
0
0.0
0.2
0.4
0.6
0.8
1.0
Relative Humidity
Desorption (23°C)
Adsorption (23°C)
Desorption (45°C)
Adsorption (45°C)

Figure 2

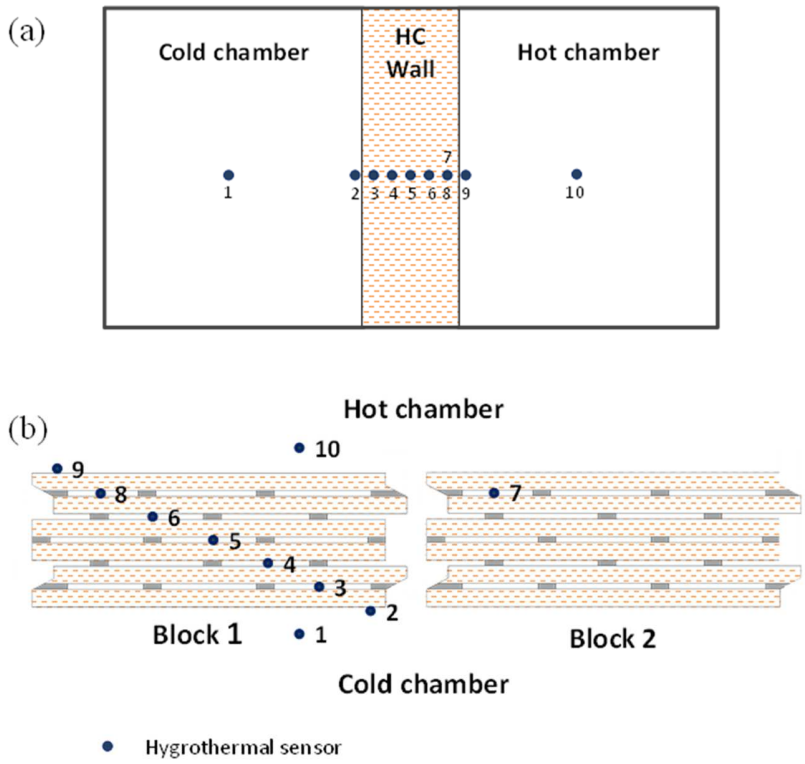
(a)
Cold chamber
HC
Wall
Hot chamber
1
2
3
4
5
6
8
7
9
10
(b)
Hot chamber
10
9
8
6
5
4
3
2
7
Block 1
1
Block 2
Cold chamber
Hygrothermal sensor

Figure 3

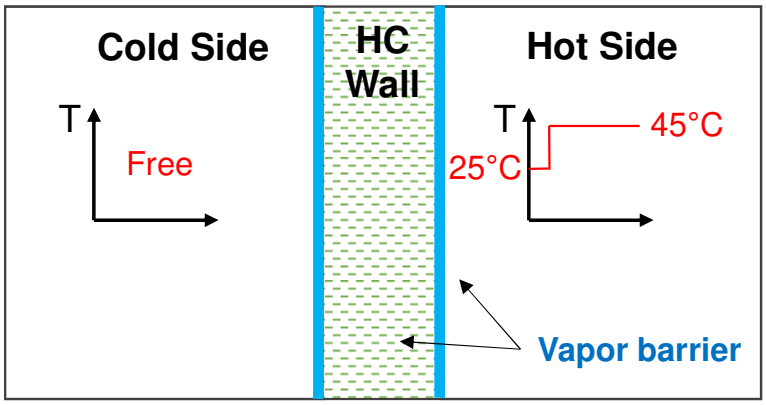
Cold Side
HC Wall
Hot Side
T
Free
T
45°C
25°C
Vapor barrier

(a)

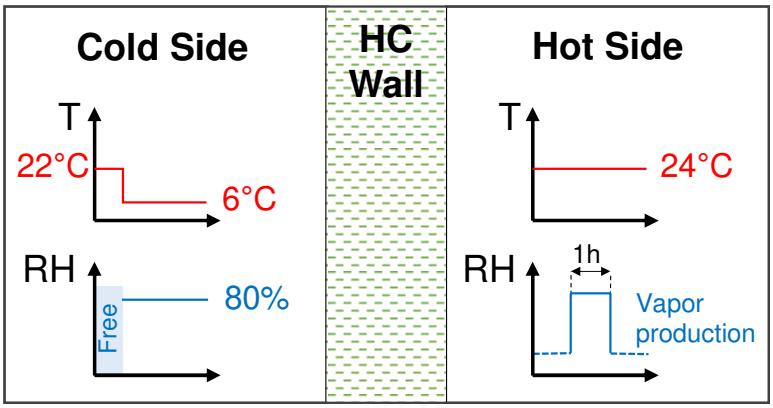
Cold Side
HC Wall
Hot Side
T
22°C
6°C
T
24°C
RH
Free
80%
RH
1h
Vapor production

(b)

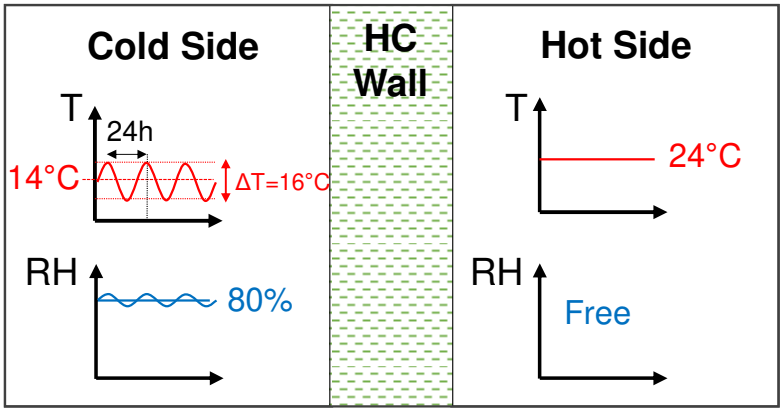
Cold Side
HC Wall
Hot Side
T
24h
14°C
ΔT=16°C
T
24°C
RH
80%
RH
Free

(c)

Figure 4

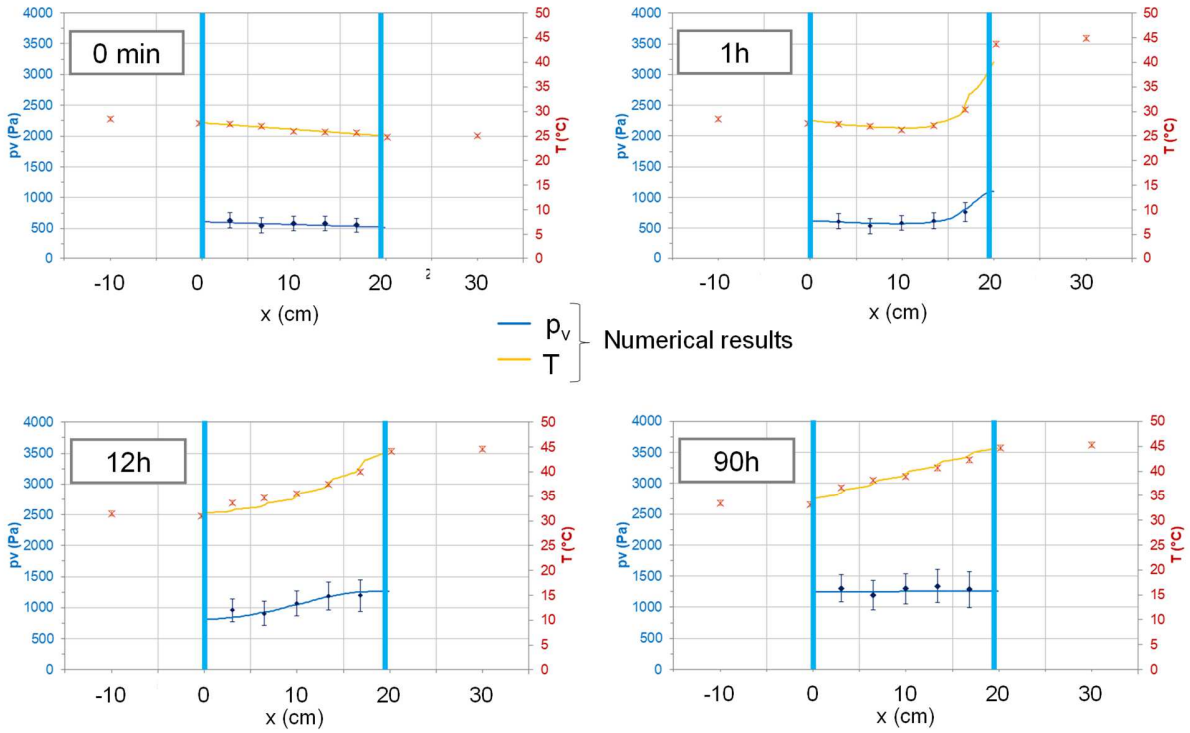

Figure 5

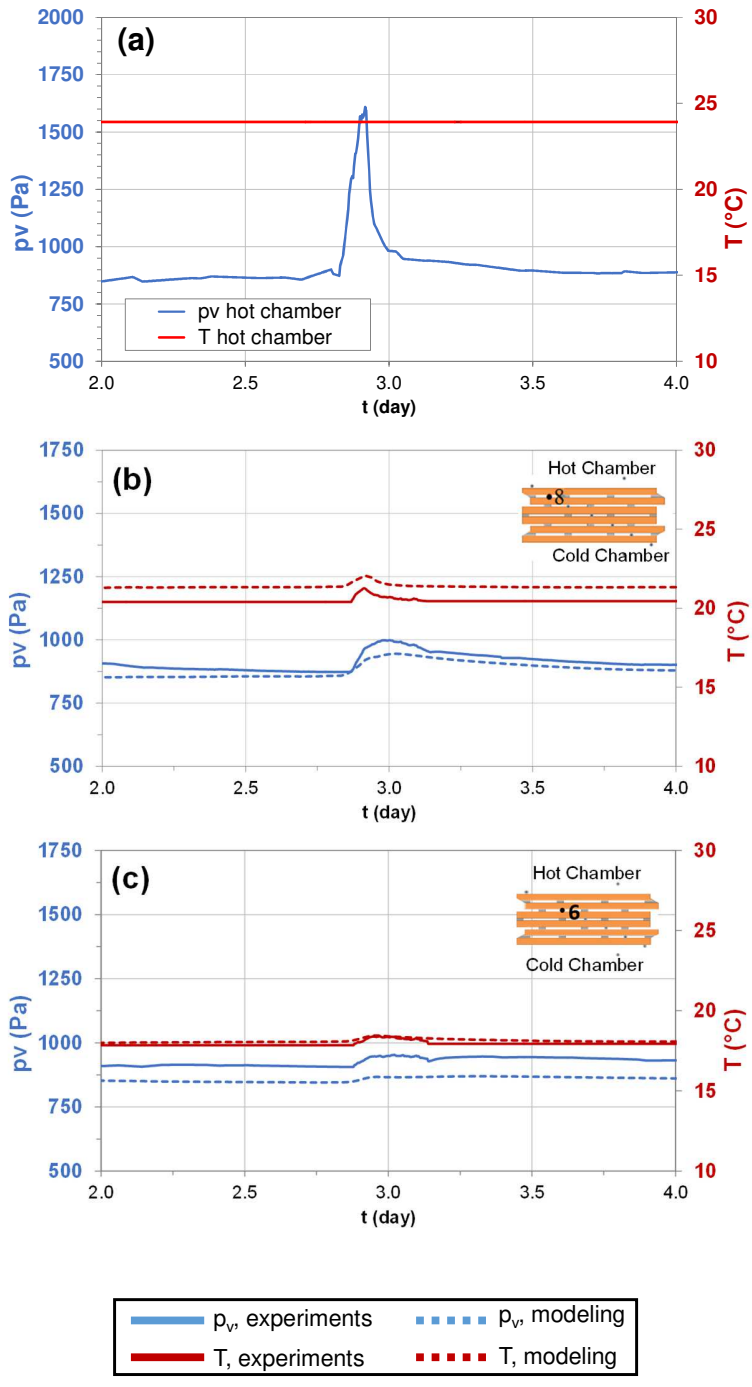
(a)
pv hot chamber
T hot chamber
pv (Pa)
T (°C)
t (day)
(b)
Hot Chamber
8
Cold Chamber
(c)
Hot Chamber
6
Cold Chamber
p_v, experiments
p_v, modeling
T, experiments
T, modeling

Figure 6

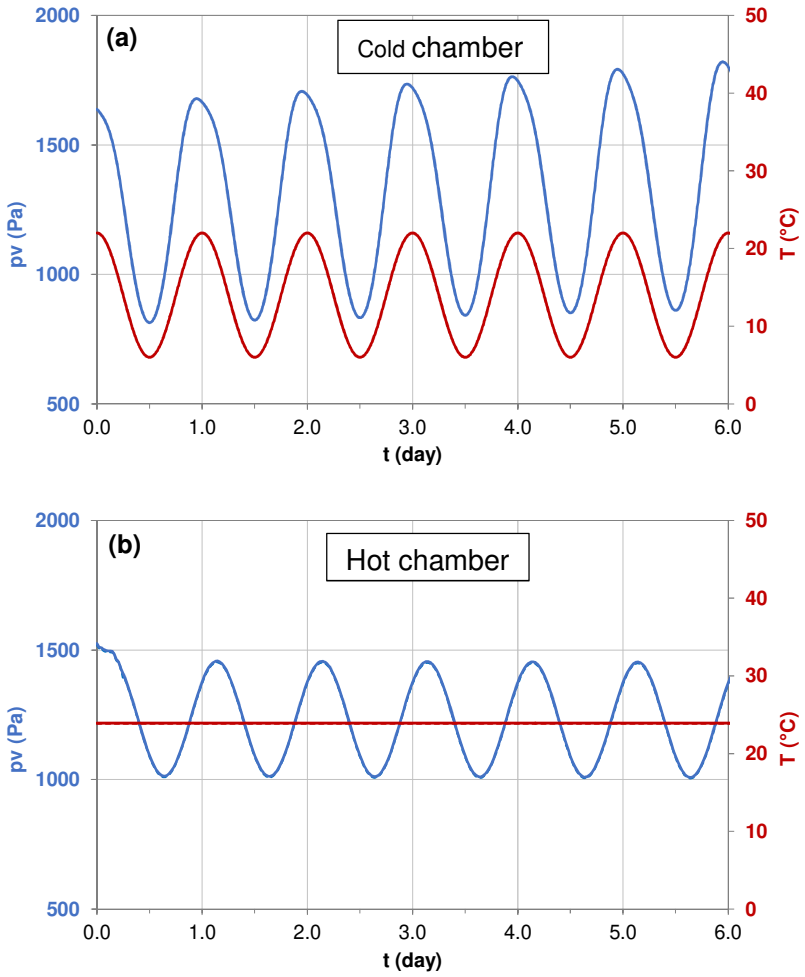
(a)
Cold chamber
2000
1500
1000
500
pv (Pa)
50
40
30
20
10
0
T (°C)
0.0
1.0
2.0
3.0
4.0
5.0
6.0
t (day)
(b)
Hot chamber
2000
1500
1000
500
pv (Pa)
50
40
30
20
10
0
T (°C)
0.0
1.0
2.0
3.0
4.0
5.0
6.0
t (day)

Figure 7

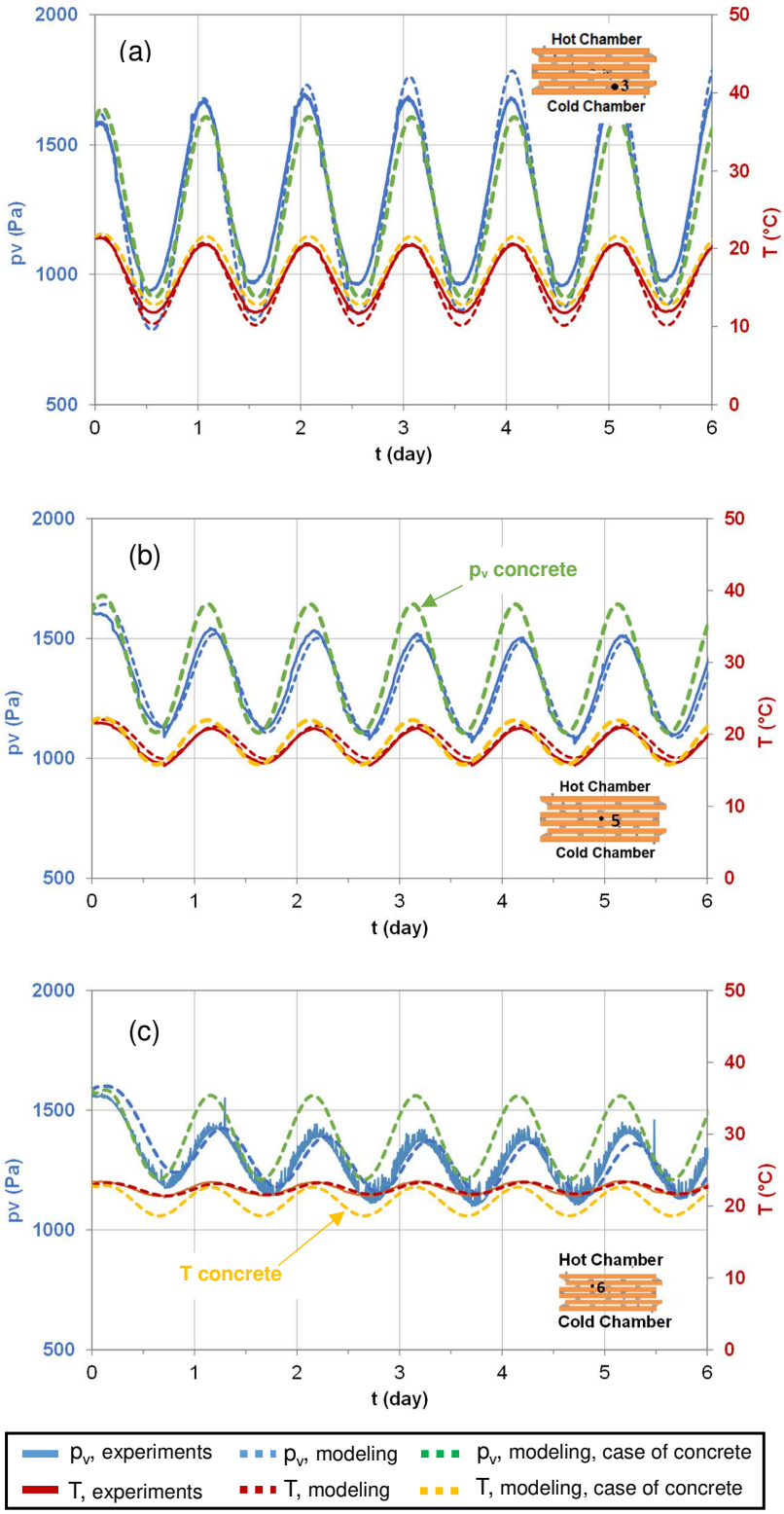
(a)
Hot Chamber
3
Cold Chamber
pv (Pa)
T (°C)
t (day)
(b)
pv concrete
Hot Chamber
5
Cold Chamber
pv (Pa)
T (°C)
t (day)
(c)
T concrete
Hot Chamber
6
Cold Chamber
pv (Pa)
T (°C)
t (day)
pv, experiments
pv, modeling
pv, modeling, case of concrete
T, experiments
T, modeling
T, modeling, case of concrete

Figure 8